Magn Reson Mater Phy (2012) 25:95–101
DOI 10.1007/s10334-011-0302-7

RESEARCH ARTICLE

Blind detection of vascular sources and territories using random vessel encoded arterial spin labeling

Eric C. Wong · Jia Guo

Received: 14 August 2011 / Revised: 22 December 2011 / Accepted: 26 December 2011 / Published online: 10 January 2012

Abstract
Object The goal of this work is to use vessel encoded arterial spin labeling (VEASL) methods to detect feeding arteries without prior knowledge of their positions, and map the vascular territory of each.
Materials and methods Five healthy subjects were scanned, each with four different tagging planes. The VEASL tagging method was modified to use 60 different pairs of encoding steps with random orientation and spacing. A signal model was developed to calculate the theoretical ASL signal resulting from a vessel in any position in the tagging plane. For each voxel, the location of the feeding vessel was estimated by finding the theoretical signal that correlates most closely with the data.
Results The main intracranial arteries, including carotid, vertebral, basilar, and cerebral arteries above the Circle of Willis were identified and localized from the ASL data in all subjects. In addition, external carotid branches were detected in all subjects.
Conclusions Randomly encoded VEASL provides data that allows for blind detection of source vessels. This method simplifies the VEASL prescription process and allows for efficient detection of atypical or collateral circulation.

E. C. Wong (✉)
Departments of Radiology and Psychiatry, UCSD Center for Functional MRI, 9500 Gilman Drive, MC 0677, La Jolla, CA 92093-0677, USA
e-mail: ecwong@ucsd.edu

J. Guo
Department of Bioengineering, University of California, San Diego, CA, USA

Keywords Magnetic resonance imaging · Stroke · Collateral circulation · Cerebral arteries · Cerebrovascular circulation

Introduction

For most ASL methods, the primary goal is to provide accurate and robust measures of perfusion. However, through manipulation of the tagging process, ASL can be extended to provide additional information on which source vessels supply which target tissues. This information, which is typically in the form of vascular territory maps, may be useful for applications such as the evaluation of stroke, risk assessment in cerebrovascular disease, and planning of treatment for tumors. ASL-based territory mapping methods include some which apply ASL tags to single vessels [1–3], and others which encode the tagging process for two or more feeding arteries such that multiple vascular territories can be decoded and mapped simultaneously [4–6]. One of these methods is vessel encoded arterial spin labeling (VEASL) [5], in which pseudo-continuous ASL (PCASL) tagging [7] is used with additional gradient pulses applied across the tagging plane to encode the ASL data with information about the location of the feeding arteries. As originally described, VEASL requires prior knowledge of the locations of vessels to be tagged in order to prescribe a series of Hadamard encoding steps across the source vessels. This in turn necessitates the collection of an angiogram, and user input or an automated algorithm for detection of vessel locations in the tagging plane. In an effort to automate the scan prescription process, Gevers et al. introduced a planning-free VEASL method [8] that uses a small number of generically defined encoding steps, and demonstrated repeatable detection of

flow territories using this approach. We explore here the use of a large number of random encoding steps to not only map vascular territories without planning, but to also uniquely identify the locations of the source arteries in the tagging plane. This provides the opportunity to identify collateral or atypical routes of circulation that may not previously be known, and may be clinically relevant.

In addition to the positions of feeding arteries, resonance offsets at the locations of the arteries in the tagging plane can also significantly affect the tagging efficiency, and methods have been proposed to either measure and correct for these offsets [9, 10] or to reduce sensitivity to them using multiphase PCASL [11]. The randomly encoded method proposed here allows for efficient estimation of both the locations and resonance offsets of feeding arteries without prior knowledge of either. Portions of this work were presented in abstract form in [12].

Materials and methods

In the original implementation of VEASL, transverse gradient pulses of alternating sign were used between RF pulses to provide vessel encoding. In the presence of resonance offsets in the tagging plane, this approach results in decreased tagging efficiency, as shown in Fig. 1a. These curves were calculated by Bloch simulation, assuming a range of flow velocities uniformly distributed from 5 to 40 cm/s in the direction of the tagging gradients, the RF and gradient parameters given below, an assumed T_2 of 200 ms for arterial blood, and neglecting T_1 decay. We note that using unipolar transverse gradient pulses for vessel encoding can provide similar encoding functionality, but with two differences [12]. First, the tagging curve as a function of the location between fully inverted and unperturbed vessels has a different shape (Fig. 1b). This curve is very well fit using three Fourier coefficients, and is given by:

$$\Delta M_Z = 2.092\,cos(\theta) - 0.322\,cos(3\theta) + 0.053\,cos(5\theta),$$

where θ is the phase along the periodic function. SNR efficiency in VEASL can be calculated using Equation 4 of [5], and is maximized using Hadamard encoding. Because the unipolar encoding curve of Fig. 1b is more weighted towards ± 1 than that of bipolar encoding (Fig. 1a), unipolar encoding more closely approximates Hadamard encoding steps, and the overall SNR is higher. Second, for unipolar encoding, resonance offsets at the tagging location result in a simple shift in the tagging curve, which does not affect the overall tagging efficiency and SNR, as opposed to the decrease in tagging efficiency that is seen with resonance offset in the bipolar case (Fig. 1). For these reasons we are currently using the unipolar approach. In order for the RF pulses to follow the phase of the spins in a vessel to be inverted, the additional phase ϕ_i (described in [5]) is given by $\phi_i = i\pi a/\lambda$, where i is the pulse number, a is the projection of the vector from isocenter to the vessel onto the direction of encoding (see [5]), and λ is encoding wavelength. For the original alternating gradient method, $\phi_i = (i\%2)\pi a/\lambda$, where % represents the integer modulus function.

Five healthy subjects were studied in a General Electric MR750 3T scanner, using a commercial 8-channel head RF coil, under a protocol approved by the local IRB. MR angiograms were acquired and were used to select the four tagging planes shown in Fig. 2. Location A features a trapezoidal arrangement of internal carotid and vertebral arteries, has relatively straight arterial segments, and allows for the possibility of separately tagging the two vertebral arteries. Location B has an anatomically very consistent arrangement of carotid and basilar arteries, but has tortuous segments nearby and typically large resonance offsets. Locations C and D are two candidate locations for tagging above the Circle of Willis (CoW) that may allow for tagging of anterior, middle, and posterior cerebral arteries. Between these two locations the anterior cerebral artery runs nearly straight posterior-anterior and is difficult to tag.

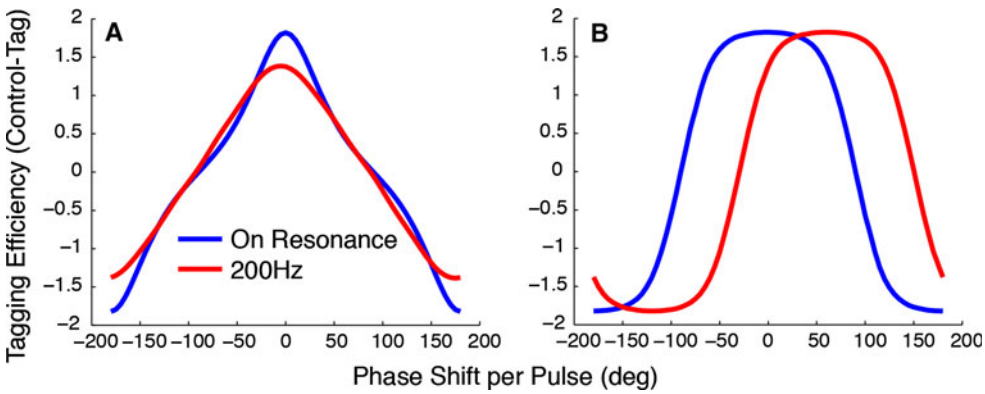

Fig. 1 Calculated VEASL signal as a function of transverse gradient induced phase shift per pulse. **a** Bipolar gradient pulses; **b** Unipolar pulses used in this study. A resonance offset at the tagging location results in reduced tagging efficiency for the bipolar pulse train, but a simple shift without amplitude reduction for the unipolar pulse train

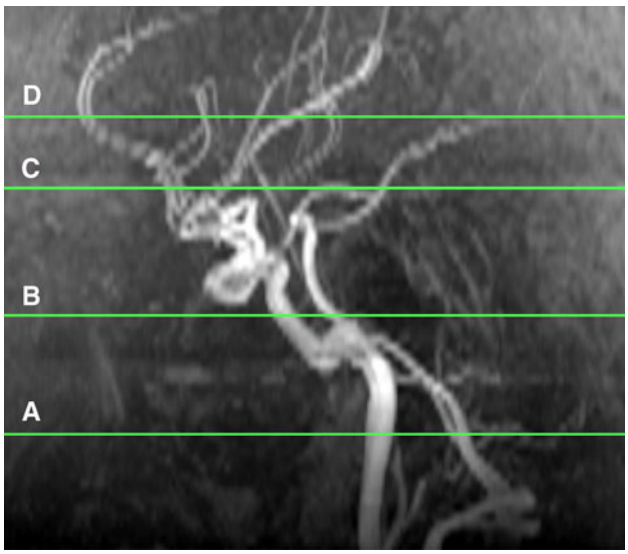

Fig. 2 Tagging planes superimposed on a sagittal projection of an MR angiogram. *A* Trapezoidal arrangement of internal carotid and vertebral arteries; *B* Triangular arrangement of internal carotid and basilar arteries at the level of the sphenoid sinus; *C* and *D* Above the Circle of Willis, allowing tagging of anterior and posterior cerebral arteries, and branches of the middle cerebral artery

At each of these tagging locations, the same 60 pairs of encoding steps were acquired, with random orientation, random phase θ, and random wavelength λ ranging from 15 to 85 mm, in addition to two pairs of non-vessel encoded steps for a total of 124 TR periods per scan. The random encoding steps were generated once and the same encodings used for every subject. The actual encodings used are available at http://cfmriweb.ucsd.edu/ecwong/public/rveasl_encodings.txt. For the second of each pair of encoding steps, the RF phase was alternated between 0 and 180° relative to the first step, such that a difference signal between the pair removes static tissue signal and leaves a symmetrical dependence of the ASL signal upon vessel location, as shown in Fig. 1b. Scan parameters were: single shot gradient echo spiral acquisition with 64^2 matrix, 22 cm FOV, nine 8 mm slices with 2 mm spacing, spatial spectral excitation, 2 μs sampling, 1.6 s tag duration, 800 μs Hamming shaped pulses with 1.4 ms spacing, tagging gradients with 8mT/m amplitude and 0.6 mT/m mean value, 1 s post labeling delay, and 3 s TR.

Images were subtracted pairwise, resulting in 61 difference images, one without transverse encoding averaged from the two pairs of non-encoded scans. For a uniform array of assumed vessel locations spanning ±64 mm with 2 mm spacing in both X and Y directions, and resonance offsets spanning ±220 Hz with 11 Hz spacing, the theoretical ASL signal across encoding steps was calculated using the random but known encoding parameters and assuming the response of Fig. 1b. This generates a matrix that maps X and Y vessel coordinates and Frequency (XYF) space into 61 dimensional ASL signal space. For each voxel in the data, the correlation coefficient (CC) between the acquired signal and the theoretical ASL signal from every XYF location was calculated, and the point in XYF space corresponding to the highest CC (CCmax) was assigned to that voxel. For this vessel detection step, images were down sampled to 32^2 using a 2×2 box shaped kernel to speed up the processing. The choice of 2 mm spacing in XY, and 11 Hz spacing in F is somewhat arbitrary. It is not the resolution in these dimensions, but simply needs to be fine enough so that correlation maxima (CCmax) in XYF space are not missed. Finer spacing than is necessary for identifying vessels is not likely to be useful, and increases computation time. Processing time for one scan (7 slices, 124 images of each) was less than one minute running in Matlab on a 8-core Linux server.

Results

A map of CCmax, and a histogram thereof are shown in Fig. 3. The histogram clearly shows a bimodal distribution, with the lower peak corresponding to areas of low or no

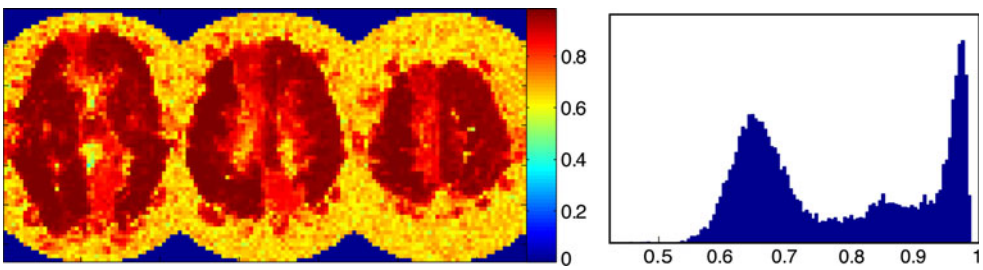

Fig. 3 Maximum correlation coefficient (CCmax) between signal from each voxel and predicted signal from any point in the XYF tagging space (see text). *Left* A map of CCmax shows high values in *gray* matter. In this subject, both the right anterior cerebral and the left posterior cerebral artery territories receive mixed supplies, and CCmax is lower in these areas. Note the high CCmax areas outside the brain, which correspond to extracranial vessels. *Right* A histogram of CCmax values shows a peak near 0.65 which corresponds to noise voxels. A CCmax threshold of 0.8 was used in this study to identify voxels that fit the signal model well, and were used to detect source vessels

perfusion (including noise outside the head), and the higher peak corresponding to voxels with high perfusion and good fit to the signal model. Voxels with CCmax >0.8 were used for estimation of vessel locations, and histograms of those voxels in XYF space were constructed. An example, with three orthogonal projections of this 3-dimensional histogram are shown in Fig. 4. Clusters in this histogram were identified manually, and the centroids of the clusters represent estimated vessel locations and resonance offsets in the tagging plane. These vessels locations were used to construct an encoding matrix and used in a linear analysis as in [5], allowing for detection and estimation of mixed supplies where they occur. In the color vascular territory maps shown, the brightness is proportional to the total flow from all feeding arteries, and the color is derived from the colors assigned arbitrarily to each vessel, mixed in RGB color space weighted by the relative contribution from each vessel.

In the example shown in Fig. 4, eight clusters are apparent in the projection of the XYF histogram onto the XY plane (Fig. 4a). The locations of these clusters are superimposed on an anatomical image of the tagging plane in Fig. 4d, and show that the central four vessels are the internal carotid and vertebral arteries. The left and right carotid arteries are designated blue and red, respectively, and the purple color of the right anterior cerebral artery territory in Fig. 4e indicates that in this subject, that territory receives a mixed supply from left and right carotids. This is consistent with data from this subject using conventional (non-random) VEASL, and MR angiography that shows a patent anterior communicating artery (data not shown). The measured resonance offsets (horizontal axis in Fig. 4b and vertical axis in Fig. 4c) are relatively small among these four vessels, ranging from −18 to 24 Hz. In addition to the four intracranial arteries, four peaks in the histogram, indicated by the arrows in Fig. 4a, presumably correspond to the temporal and occipital branches of the external carotid arteries. The vascular territories of these four arteries are indicated by arrows with corresponding colors in Fig. 4e. These territories have been increased in brightness by a factor of three for visibility, and are likely mainly cutaneous arteries, many of which are blurred by the spiral acquisition. External carotid territories were detected consistently in all scans.

Figure 5 shows the vascular territories of the intracranial arteries for all five subjects, for three of the four tagging planes. Only one of the nine slices is shown. The highest tagging plane (Fig. 2d) yielded results similar to plane c, and is not shown. In this figure, the relevant region of the tagging plane is shown below each territory map, with the XY projection of the XYF histogram overlayed on the anatomical image in magenta. Vessels locations were chosen manually at the peaks of the histogram, and are indicated by asterisks, with colors corresponding to associated

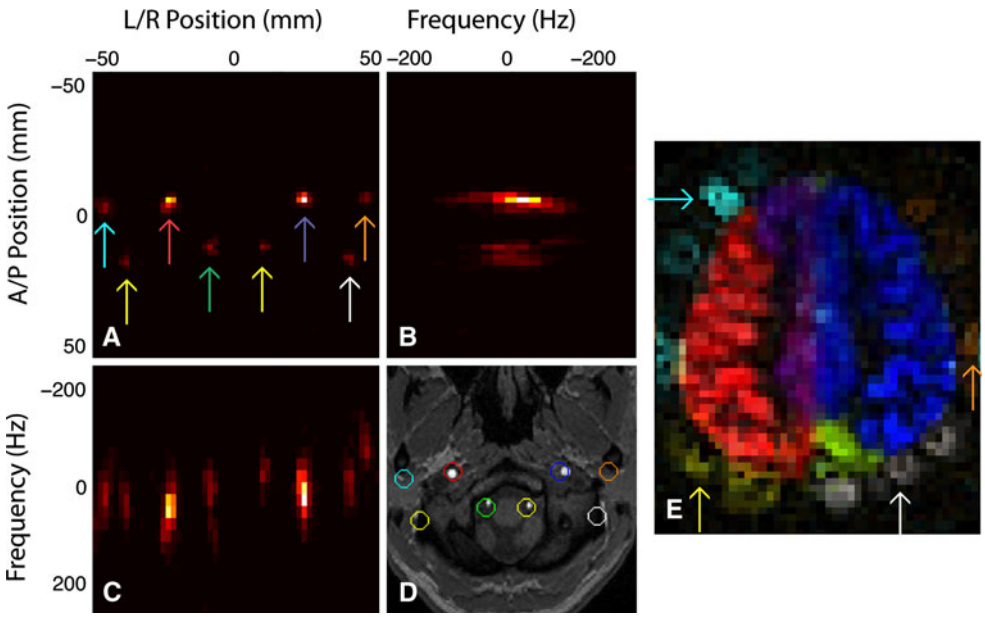

Fig. 4 Detection of source vessels. Three orthogonal projections of 3D histogram of voxels projected into XYF space (see text). **a** Projection onto XY plane; **b** Projection onto FY plane; **c** Projection onto XF plane. Peaks in these projections correspond to source vessels. **d** Eight peaks seen in **a**, shown as colored circles, superimposed on an anatomical image of the tagging plane. These eight vessels correspond to two carotid arteries, two vertebral arteries, and four extracranial arteries. **e** Territories mapped using the same color scheme as the circles in **d**, with extracranial territories increased in brightness by a factor of three for visibility. Extracranial territories were detected in all subjects, and are indicated by arrows. Right anterior cerebral territory receives mixed left and right carotid contributions, resulting in a *purple color* (a mix of *red* and *blue*)

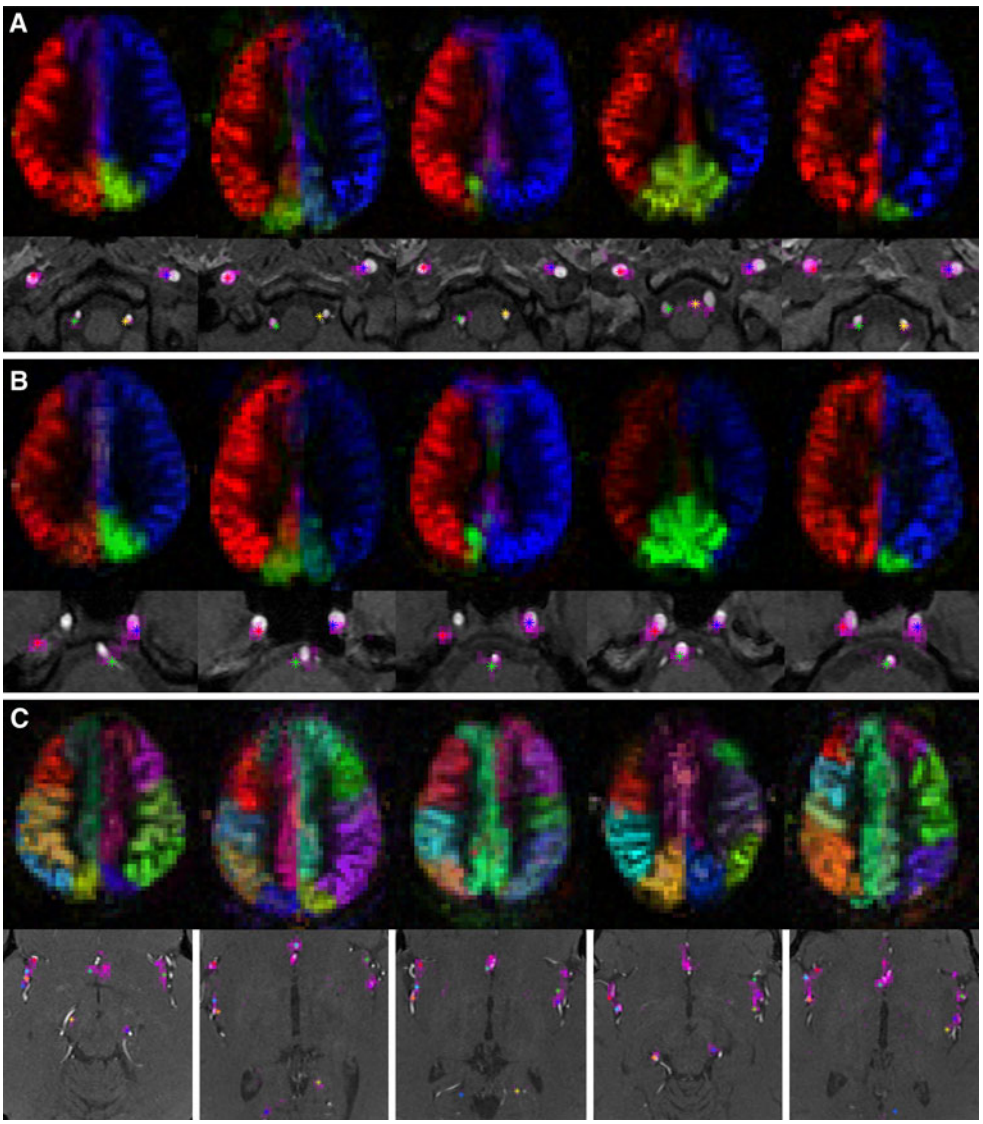

Fig. 5 Source vessels and vascular territories for all 5 subjects (*left to right*). *From Top* tagging planes **a**, **b**, and **c** (see Fig. 2). Below each territory map, an anatomical image of the tagging plane is shown, with a projection of the histogram in XYF space superimposed in magenta. Peaks in this histogram are identified with colored asterisks, with colors corresponding to the vascular territory map

vascular territory. In all subjects, separate peaks in the histogram corresponding to left and right vertebral arteries were seen (top row), although the number of voxels appearing at each vertebral location can be small. In row 2, subects 1 and 3, the localization of the right carotid artery was significantly off, but the nearest peak in the XY histogram did correctly identify the vascular territory. The resonance offsets at this tagging plane can be very large, as the vessels are close to the sphenoid sinus, and it was suspected that the resonance offset could affect the vessel localization. However the offsets measured at the two mislocalized carotid arteries were 21 Hz and 75 Hz, while larger offsets were measured in other subjects. For example, offsets of 214 Hz, 184 Hz, and 227 Hz were measured for subject 2 in this plane, and the localization in that subject was good. For tagging above the CoW (row 3), multiple vessels, including anterior and posterior cerebral arteries, and several branches of the middle cerebral arteries are consistently detected.

Discussion

The data shown here demonstrates that randomly encoded VEASL data can provide sufficient information to decode source vessel locations. Using a threshold on CCmax was an effective means of identifying voxels that will provide accurate vessel localization. The simple VEASL signal model used here, which assumes a single response function independent of flow velocity, is accurate enough to provide

fits to the data with CC >0.8, and often exceeding 0.95. We initially used signal variance across encodes as a parameter to select voxels for source analysis, but found that cardiac pulsations, which generate large and synchronous signal modulation across many voxels, often cluster to a spurious point in XYF space, leading to identification of a vessel that does not exist. The use of a CCmax threshold effectively reduces this problem, as we have not found vascular pulsations to pass the threshold. Because of the large number of points in XYF space ($65 \times 65 \times 41$), the CC between even pure noise and the best fitting signal model is relatively high (i.e the peak centered around 0.65 in Fig. 3). For smaller numbers of encoding steps, CCmax for noise is even higher, and was found to be 0.75 with 30 pairs of encoding steps, and 0.90 with 15 pairs of encodings. Thus, for the CCmax threshold of 0.8 used in this study, approximately 60 pairs of encoding steps (as used in this study) are required to provide a clear separation in CCmax between well perfused voxels and noise.

In areas that receive mixed supply, the VEASL signal should not correlate well with the signal model associated with any single point in XYF space. The potential for this to compromise vessel detection is clearly present when tagging the vertebral arteries, as they join to form the basilar artery prior to entering the CoW. Apparently in all five of the subjects studied, there is a sufficient lack of mixing in at least some portion of the posterior territory that both vertebral arteries could be identified. This is consistent with [13] in which a general lack of complete vertebral mixing was found, but it is not yet known whether this is reliably the case across the population.

In this work we have demonstrated that it is not necessary to identify source vessels within the tagging plane prior to VEASL scanning. However, we did use an angiogram to choose tagging planes that contain relatively straight and well separated vessel segments. A study to determine the effect of the choice of tagging plane on the effectiveness of random VEASL is currently underway. It is possible that choosing a tagging plane based on anatomical landmarks, as is commonly done for conventional PCASL, is sufficient for random VEASL, but this remains to be seen. Under most circumstances where VEASL data is of interest, an angiogram is likely to be desired as well, so it is unlikely that random VEASL would reduce the scan time per se. One goal of random VEASL is to reduce the required user input for scan prescription, which may save time, but the more important goal is to detect all source vessels. An obvious example is the detection of an external carotid collateral in a patient with cerebrovascular disease such as stroke or carotid stenosis, and it is promising that in this study, the territories of extracranial arteries were consistently detected.

The SNR efficiency of random VEASL is in principle similar to that of multiphase PCASL [11]. While multiphase PCASL uniformly samples the tagging efficiency curve of Fig. 1 to provide insensitivity to resonance offsets, random VEASL randomly samples the same curve, but with a different random sampling pattern for each point in the tagging plane. The SNR efficiency can be calculated as described in [5] for any given encoding matrix, and depends on proximity of other detected vessels. If two vessels are close to one another in XYF space, this translated into a poorly conditioned encoding matrix and noise amplification in the decoding process. For vessels that are far apart, the encoding matrix is well conditioned, and the SNR efficiency approaches the RMS value of the tagging efficiencies of the encoding steps. For conventional PCASL with perfect tagging efficiency and no resonance offset the SNR efficiency is 1. If the tagging efficiency curve was a simple sinusoid, then the SNR efficiency for either densely sampled MP-PCASL or random VEASL would be $1/\sqrt{2} = 0.707$, as this is the RMS value of a sin function. For the calculated curve of Fig. 1b, the RMS value is slightly higher (0.74), which is identical to the SNR efficiency calculated through the decoding matrix for distant vessels. Our preliminary calculations show that the SNR efficiency falls to half of this value (0.37) due to noise amplification when two vessels are 6 mm apart. More complete characterization of the SNR behavior of random VEASL is currently underway.

Localization of the decoded vascular sources was accurate in most but not all cases. In particular, the localization of the right internal carotid at the level of the sphenoid sinus in subjects 1 and 3 was significantly off, and the cause of this is currently under investigation.

The vessel locations in this study were chosen by hand at the local peaks of the histogram of voxels in XY tagging plane space. For most of the cases, particularly below the CoW, a simple threshold detected the same vessel locations, but above the CoW the identification of vessels is more uncertain. The automation of vascular territory detection is an important next step in this line of work, as it would more fully realize the potential of automated vascular territory mapping without a priori knowledge of vessel locations. Approaches of interest include clustering methods [14, 15] in any combination of three spaces: physical brain space, as territories tend to be contiguous in the brain; raw data space, where the noise often has predictable characteristics; and XYF tagging plane space, where the vessels are inherently sparse. Bayesian estimation methods have also been applied with success to the general problem of VEASL data processing [16, 17], and can be adapted to the methods described here. The authors are willing to share the raw data from this study with researchers who are interested in developing or testing algorithms for improved detection of vessels and/or mapping of territories.

Conclusion

We have demonstrated here that randomly encoded VEASL allows for the unique identification of source vessel locations and resonance offsets. We expect that this new method may provide important and specific information for the diagnosis and management of cerebrovascular disease, tumors, and other conditions where collateral or aberrant flow patterns may be present and it is important to identify the arterial supply.

Acknowledgments This work was supported by Grant R01 EB002096 from the National Institutes of Health.

References

1. Davies NP, Jezzard P (2003) Selective arterial spin labeling (SASL): perfusion territory mapping of selected feeding arteries tagged using two-dimensional radiofrequency pulses. Magn Reson Med 49(6):1133–1142
2. Werner R, Norris DG, Alfke K, Mehdorn HM, Jansen O (2005) Continuous artery-selective spin labeling (CASSL). Magn Reson Med 53(5):1006–1012
3. Helle M, Norris DG, Rufer S, Alfke K, Jansen O, van Osch MJ (2010) Superselective pseudocontinuous arterial spin labeling. Magn Reson Med 64(3):777–786
4. Gunther M (2006) Efficient visualization of vascular territories in the human brain by cycled arterial spin labeling MRI. Magn Reson Med 56(3):671–675
5. Wong EC (2007) Vessel encoded arterial spin labeling using pseudo-continuous tagging. Magn Reson Med 58(6):1086–1091
6. Zimine I, Petersen ET, Golay X (2006) Dual vessel arterial spin labeling scheme for regional perfusion imaging. Magn Reson Med 56(5):1140–1144
7. Dai W, Garcia D, de Bazelaire C, Alsop DC (2008) Continuous flow-driven inversion for arterial spin labeling using pulsed radio frequency and gradient fields. Magn Reson Med 60(6):1488–1497
8. Gevers S, Bokkers RP, Hendrikse J, Majoie CB, Kies DA, Teeuwisse WM, Nederveen AJ, van Osch MJ (2011) Robustness and reproducibility of flow territories defined by planning-free vessel-encoded pseudocontinuous arterial spin-labeling. Am J Neuroradiol. doi:10.3174/ajnr.A2410
9. Jung Y, Rack-Gomer A, Wong E, Buracas G, Liu T (2009) Pseudo-continuous arterial spin labeling with optimized tagging efficiency for quantitative ASL fMRI. In: Proceedings 17th scientific meeting, ISMRM, Honolulu, p 1578
10. Jahanian H, Noll DC, Hernandez-Garcia L (2011) B(0) field inhomogeneity considerations in pseudo-continuous arterial spin labeling (pCASL): effects on tagging efficiency and correction strategy. NMR Biomed. doi:10.1002/nbm.1675
11. Jung Y, Wong EC, Liu TT (2010) Multiphase pseudocontinuous arterial spin labeling (MP-PCASL) for robust quantification of cerebral blood flow. Magn Reson Med 64(3):799–810
12. Wong EC, Guo J (2011) Blind detection of source vessel locations and resonance offsets using randomly encoded VEASL. In: Proceedings 19th scientific meeting, ISMRM, Montreal, p 294
13. Kansagra AP, Wong EC (2008) Mapping of vertebral artery perfusion territories using arterial spin labeling MRI. J Magn Reson Imaging 28(3):762–766
14. Kansagra A, Wong E (2009) Automated segmentation of multiple vascular territories from vessel encoded pseudo-continuous arterial spin labeling MRI data. In: Proceedings 17th scientific meeting, ISMRM, Honolulu, p 3652
15. Wong E, Kansagra A (2008) Mapping middle cerebral artery branch territories with vessel encoded pseudo-continuous ASL: sine/cosine tag modulation and data clustering in tagging efficiency space. In: Proceedings 16th scientific meeting, ISMRM, Toronto, p 182
16. Chappell MA, Okell TW, Jezzard P, Woolrich MW (2010) A general framework for the analysis of vessel encoded arterial spin labeling for vascular territory mapping. Magn Reson Med 64(5):1529–1539
17. Chappell MA, Okell TW, Jezzard P, Woolrich MW (2009) Vascular territory image analysis using vessel encoded arterial spin labeling. Med Image Comput Comput Assist Interv 12(Pt 2):514–521